1   **Modelling of sediment transport and bed deformation in rivers with continuous bends**[*]

2   *Hefang Jing[a†] Chunguang Li[a] Yakun Guo[b] Lixiang Zhang[c] Lijun Zhu[d] Yitian Li[e]*

3   [a] Res. Inst. Numer. Comput. & Eng. Appl., Beifang University of Nationalities, Yinchuan 750021, China.
4   [b] School of Engineering, University of Aberdeen, Aberdeen, AB24 3UE, UK.
5   [c] Department of Engineering Mechanics, Kunming University of Science and Technology, Kunming, 650051,
6   China.
7   [d] School of Information and Computing Science, Beifang University of Nationalities, Yinchuan 750021, China.
8   [e] State Key Laboratory of Water Resources and Hydropower Engineering Sciences, Wuhan University, Wuhan
9   430072, China.
10

11   Abstract

12   A two dimensional (2D) RNG k-ε sediment model including the effects of secondary currents is

13   developed to simulate sediment transport and bed deformation in rivers with continuous bends.

14   Nonuniform suspended and bedload sediment transports and variation of effective bed material

15   size distribution are included in the model. A semi-coupled scheme for sediment model is

16   proposed, which can be used for simulating both the long- and short-term sediment transport

17   whenever riverbed changes. The model is applied to simulate the flow and sediment transport in

18   the Shapotou reservoir in the upper reach of the Yellow River which is a typical natural river reach

19   with continuous bends. River bed deformations caused by suspended and bedload sediment

20   transport are investigated. Good agreement between the numerically simulated results and the field

21   measurements is obtained, indicating that the model is capable of simulating the sediment

22   transport and predicting the bed deformation of rivers having continuous bends with reasonable

23   accuracy.

24   **Key words：** RNG k-ε turbulence model, bed deformation，suspended sediment, bedload sediment,

25   bed material granularity

NOMENCLATURE			
C	Chezy coefficient	h	water depth
D_{50}	medium diameter of bed material	k	turbulent kinetic energy
P_{mL}	bed material granularity	n	Manning coefficient
$P_{mL,0}$	original bed material granularity	u	velocity in x direction
S	sediment concentration	v	velocity in y direction
S_L	group sediment concentration	z	water level
S_v	sediment concentration by volume	α_L	group saturation recovery coefficient of sediment
S^*	sediment carrying capacity	γ	water specific gravity
S_L^*	group sediment carrying capacity	γ'	dry specific gravity of sediment
$\overline{U}$	depth averaged velocity	κ	Karman constant
Z	bed elevation	ε	turbulence dissipation rate
$Z_{S,L}$	the deposition thickness of the L-th group suspended sediment	v	water viscosity
$Z_{b,L}$	the deposition thickness of the L-th group bedload	v_t	water eddy viscosity
d_{50}	medium diameter of suspended sediment	γ_s	sediment specific gravity
d_m	averaged diameter of suspended sediment	γ_m	Specific gravity of muddy water
d	diameter of sediment	ω	sediment settling velocity
g	gravity acceleration	ω_L	sediment settling velocity of the L-th group sediment

26

27   **1. Introduction**

28   Flow and sediment transport near hydraulic structures in rivers have been extensively studied

29   using various approaches, such as theoretical analysis, laboratory experiments, field measurements

30   and numerical simulation. Among these approaches, numerical simulation has advantages in

31   several aspects and has been increasingly used (Falconer 1992; Guo *et al.* 2007). In natural rivers,

32   horizontal scale is usually much greater than vertical scale; therefore, it is suitable to apply depth

33   averaged two dimensional (2D) models (Guo *et al.* 2012). Generally speaking, numerical

34   simulation using these models not only requires less computational time than three dimensional

35   (3D) sediment models (particularly for large scale simulation), but also is more accurate than that

36   of 1D sediment models. As a result, depth averaged 2D sediment models are widely applied in

37   engineering to study sediment transport and river bed deformation. Nagata *et al.* (2000) developed

38   a 2D sediment model for inviscid river banks. Hung *et al.* (2009) developed an unsteady 2D

39   depth-averaged model for nonuniform sediment transport in alluvial channels, taking the transport

40   mechanisms of cohesive and noncohesive sediment, suspended sediment and bedload into account.

41   Duan and Julien (2010) conducted 2D numerical simulation for a laboratory bend, considering

42   transport of suspended sediment and bedload, and river bed deformation. Li and Millar (2011)

43   developed a 2D morphodynamic model of gravel-bed river with floodplain vegetation, considering

44   the effects of riparian and floodplain vegetation on bank strength, floodplain flow resistance, shear

45   stress partitioning, and bedload transport. Serrano-Pacheco *et al.* (2012) conducted 2D bedload

46   transport simulations, in which bedload transport is governed by a power law of flow velocity and

47   by a flow/sediment interaction parameter.

48

49   Though these 2D sediment models have been widely used to simulate the sediment transport and

50   bed deformation in rivers and open channels, many of them are either laminar model, or zero

51   equation turbulent model or standard k-ε turbulent model. As such, they cannot be applied to

52   simulate the complicated turbulent flow and sediment transport in rivers with continuous bends in

53   which the effect of secondary currents induced by the bends or curved channels is important.

54   Some models were modified and taken the effect of secondary currents into account, but they can

55   only be applied to simulate the regular bends in laboratory open channels, and are difficult to be

56   applied to simulate the flow and sediment transport in natural rivers with continuous bends under

57   investigation. Therefore, these 2D sediment models need to be improved before they can be

58   applied to simulate the natural rivers with continuous curves.

59

60   The RNG k-ε model, developed from standard k-ε model (Versteeg and Malalasekera,1995), has

61   the advantages over the standard k-ε model. For example, it is more accurate by adding an extra

62   term in the ε-equation; can be used to simulate the turbulent eddy with high accuracy and is

63   applicable to simulate the flows of both the high and low Reynolds number (Jing et al. 2009,

64   2011). In this study, a 2D depth averaged RNG k-ε sediment model is developed to simulate the

65   flow and sediment transport in the Shapotou reservoir at the upper reach of the Yellow River with

66   continuous bends. The effect of secondary current on flow transport is taken into account in the

67   turbulent model. Both the non-uniform suspended and non-uniform bedload sediment transport is

68   included in the model. In addition, the variation of size distribution of effective bed materials is

69   also simulated in the model. Depth averaged velocity, water level, transport of suspended

70   sediment and bed deformation caused by suspended and bedload sediment transports are

71   investigated.

72

73   The governing equations of sediment models can be divided into two modules: flow module and

74   sediment module. The first module includes flow continuous equation, momentum equations and

75   turbulence equations, while the second module includes transportation equations of suspended

76 sediment and bedload and bed deformation equations. Therefore, there are two basic schemes to

77 numerically solve sediment models, i.e. coupled scheme and decoupled scheme. In the coupled

78 scheme, the flow and sediment modules are solved simultaneously, while in the decoupled scheme,

79 the flow module is solved first, then the sediment module. In other words, in the decoupled

80 scheme, the flow module will no longer be run after the sediment module starts. Generally

81 speaking, the coupled scheme is suitable for short time numerical simulation with the rapid change

82 of the river bed. It is usually not suitable for long time numerical simulation of sediment transport

83 due to the large CPU time consuming. On the other hand, the decoupled scheme is suitable for

84 long time numerical simulation with the slow variation of river bed as it requires less computing

85 time. Usually, the hydraulic elements, such as water level and velocity, change very slightly in the

86 long time numerical simulation of sediment transport when river bed changes slowly. In this

87 situation, it is not necessary to calculate the flow module every time step from the point of view of

88 computing cost. However, after a certain time steps of running the sediment module, the river bed

89 deformation accumulates to a degree that can significantly affect the flow elements. In this

90 situation, the flow module needs to be run to account the effect of sediment transport and bed

91 deformation on the flow field. However, in the decoupled scheme, the flow module is stopped

92 forever after sediment module begins to run. Therefore, the decoupled scheme is unreasonable and

93 needs to be improved in order to simulate the effect of the sediment transport on the flow field.

94 This is one of the motivations of this work in which a semi-coupled scheme is developed by

95 combining the advantages of coupled and decoupled schemes. In the proposed scheme, the

96 sediment module keeps running, while the flow module runs intermittently. Therefore, the scheme

97 is efficient and is less time consuming than the coupled scheme and is more accurate than the

98   decoupled scheme. The semi-coupled scheme is not only suitable for simulating both the long and

99   short time sediment transport, but is also capable of treating both the rapid and slow change of the

100   river bed.

101

102   **2. Mathematical model**

103   *2.1. The 2D depth averaged RNG k-ε model in Cartesian coordinate*

104   The 2D depth averaged RNG *k-ε* sediment model includes two basic modules: hydraulic module

105   and sediment module. The hydraulic module consists of the following equations (Versteeg and

106   Malalasekera, 1995; Duan and Nanda 2006; Serrano-Pacheco, *et al.* 2012):

107
$$\frac{\partial z}{\partial t} + \frac{\partial (hu)}{\partial x} + \frac{\partial (hv)}{\partial y} = 0 \tag{1}$$

108
$$\frac{\partial (hu)}{\partial t} + \frac{\partial (huu)}{\partial x} + \frac{\partial (huv)}{\partial y} = \frac{\partial}{\partial x}\left(v_e h \frac{\partial u}{\partial x}\right) + \frac{\partial}{\partial y}\left(v_e h \frac{\partial u}{\partial y}\right) - gh\frac{\partial z}{\partial x} - \frac{gn^2 u\sqrt{u^2+v^2}}{h^{1/3}} \tag{2}$$

109
$$\frac{\partial (hv)}{\partial t} + \frac{\partial (hvu)}{\partial x} + \frac{\partial (hvv)}{\partial y} = \frac{\partial}{\partial x}\left(v_e h \frac{\partial v}{\partial x}\right) + \frac{\partial}{\partial y}\left(v_e h \frac{\partial v}{y}\right) - gh\frac{\partial z}{\partial y} - \frac{gn^2 v\sqrt{u^2+v^2}}{h^{1/3}} \tag{3}$$

110
$$\frac{\partial (hk)}{\partial t} + \frac{\partial (huk)}{\partial x} + \frac{\partial (hvk)}{\partial y} = \frac{\partial}{\partial x}\left(\alpha_k v_e h \frac{\partial k}{\partial x}\right) + \frac{\partial}{\partial y}\left(\alpha_k v_e h \frac{\partial k}{\partial y}\right) + h(P_k + P_{kv} - \varepsilon) \tag{4}$$

111
$$\frac{\partial (h\varepsilon)}{\partial t} + \frac{\partial (hu\varepsilon)}{\partial x} + \frac{\partial (hv\varepsilon)}{\partial y} = \frac{\partial}{\partial x}\left(\alpha_\varepsilon v_e h \frac{\partial \varepsilon}{\partial x}\right) + \frac{\partial}{\partial y}\left(\alpha_\varepsilon v_e h \frac{\partial \varepsilon}{\partial y}\right) + h\left[\frac{\varepsilon}{k}(C_{1\varepsilon}^* P_k - C_{2\varepsilon}\varepsilon) + P_{\varepsilon v}\right]$$

112
$$\tag{5}$$

113

114   And the sediment module includes the following equations:

115
$$\frac{\partial hS_L}{\partial t} + \frac{\partial huS_L}{\partial x} + \frac{\partial hvS_L}{\partial y} = \frac{\partial}{\partial x}\left(v_e h \frac{\partial S_L}{\partial x}\right) + \frac{\partial}{\partial y}\left(v_e h \frac{\partial S_L}{\partial y}\right) - \alpha_L \omega_L (S_L - S_L^*) \tag{6}$$

116
$$\gamma_s' \frac{\partial Z_{S,L}}{\partial t} = \alpha_L \omega_L (S_L - S_L^*) \tag{7}$$

$$\gamma'_s \frac{\partial Z_{b,L}}{\partial t} + \frac{\partial g_{bx,L}}{\partial x} + \frac{\partial g_{by,L}}{\partial y} = 0 \tag{8}$$

117

118
$$\gamma'_s \frac{\partial E_m P_{mL}}{\partial t} + \alpha_L \omega_L (S_L - S_L^*) + \frac{\partial g_{bx,L}}{\partial x} + \frac{\partial g_{by,L}}{\partial y} + \gamma'_s [\varepsilon_1 P_{mL} + (1-\varepsilon_1)P_{mL,0}] \left(\frac{\partial z_b}{\partial t} - \frac{\partial E_m}{\partial t} \right) = 0 \tag{9}$$

119   In above equations: z=the water level; h=the water depth; u, v= the vertically averaged velocities

120   in x, y directions, respectively; t=the time; k= the turbulent kinetic energy; ε =the turbulence

121   dissipation rate; g=the acceleration of gravity; n=the Manning's coefficient; S_L, $S_L^*, \omega_L, \alpha_L$ =the

122   L-th group sediment concentration, sediment carrying capacity, settling velocity, saturation

123   recovery coefficient, respectively; $Z_{S,L}$ =the deposition thickness of the L-th group suspended

124   sediment, γ_s' =the dry specific gravity of sediment; $Z_{b,L}, g_{bx,L}$ and $g_{by,L}$ =deposition thickness,

125   discharge per unit width in x and y directions of the L-th group bed load, respectively; P_{mL} and

126    $P_{mL,0}$ =bed material granularity and original bed material granularity, respectively; z_b =the bed

127   level, E_m =the thickness of active layer; $\varepsilon_1 = 0$ (if the original river bed is scoured) or $\varepsilon_1 = 1$ (if

128   the original river bed is deposited).

129

130   In (1)-(6), the effective viscosity (v_e) is the sum of the viscosity of water (v) and the eddy

131   viscosity coefficient of water (v_t). The values and the calculation of some coefficients such as

132    $v_t, P_k, P_{kv}, P_{\varepsilon v}, C_{1\varepsilon}^*, C_\mu, \alpha_k, \alpha_\varepsilon$, can be found in (Yakhot and Orzag, 1986; Rodi 1993).

133

134   *2.2. Modified 2D depth averaged RNG k-ε model in body fitted coordinates*

135   As the river reach under investigation consists of several irregular bends where strong circulation

136   flow exists, the 2D depth averaged RNG k-ε sediment model usually can not reflect the influence

137   of such flow. Therefore, the model needs to be modified to take the influence of circulation flow

138   into account.

139

140   To facilitate the description, the general control equations of the 2D depth averaged RNG k-ε

141   sediment model is written in the body fitted coordinate system (BFC):

142    $$\frac{\partial}{\partial t}(h\Phi) + \frac{1}{J}\frac{\partial}{\partial \xi}(hU\Phi) + \frac{1}{J}\frac{\partial}{\partial \eta}(hV\Phi) = \frac{1}{J}\frac{\partial}{\partial \xi}(\frac{\alpha h\Gamma_\Phi}{J}\frac{\partial \Phi}{\partial \xi}) + \frac{1}{J}\frac{\partial}{\partial \eta}(\frac{\gamma h\Gamma_\Phi}{J}\frac{\partial \Phi}{\partial \eta}) + S_\Phi(\xi,\eta) \quad (10)$$

143   where general variable Φ represents 1, u, v, k, ε, S_L in (1)-(6), respectively; ξ and η = the

144   curvilinear coordinates along river bank direction and perpendicular to the river bank direction,

145   respectively; J, α, β, γ = transformation factors, $J = x_\xi y_\eta - x_\eta y_\xi$, $\alpha = x_\eta^2 + y_\eta^2$,

146    $\beta = x_\xi x_\eta + y_\xi y_\eta$, $\gamma = x_\xi^2 + y_\xi^2$; U and V = components of inverter velocity in ξ and η

147   directions, respectively, $U = uy_\eta - vx_\eta$, $V = -uy_\xi + vx_\xi$; Γ_Φ = general diffusion coefficient;

148   the source terms of the momentum equations (Eq.s (2) and (3)) are as following:

149    $$S_u = -\frac{1}{J}gh(z_\xi y_\eta - z_\eta y_\xi) - \frac{1}{J}\frac{\partial}{\partial \xi}\left(\frac{\beta\Gamma_u h}{J}\frac{\partial u}{\partial \eta}\right) - \frac{1}{J}\frac{\partial}{\partial \eta}\left(\frac{\beta\Gamma_u h}{J}\frac{\partial u}{\partial \xi}\right) - \frac{gn^2 u\sqrt{u^2+v^2}}{h^{1/3}} \quad (11)$$

150    $$S_v = -\frac{1}{J}gh(-z_\xi x_\eta + z_\eta x_\xi) - \frac{1}{J}\frac{\partial}{\partial \xi}\left(\frac{\beta\Gamma_v h}{J}\frac{\partial v}{\partial \eta}\right) - \frac{1}{J}\frac{\partial}{\partial \eta}\left(\frac{\beta\Gamma_v h}{J}\frac{\partial v}{\partial \xi}\right) - \frac{gn^2 v\sqrt{u^2+v^2}}{H^{\frac{1}{3}}} \quad (12)$$

151   To simulate the influence of circulation flow of bend, extra source terms need to be added in the

152   momentum equations. These new source terms are as following (Lien, et al, 1999):

153    $$S_u^{new} = S_u + M_u , \quad S_v^{new} = S_v + M_v \quad (13)$$

154   in which the extra source terms can be calculated by

155    $$M_u = -\frac{1}{J^2}\frac{u\sqrt{\gamma}}{\sqrt{u^2+v^2}}\frac{\partial}{\partial \eta}\left(|\overline{u}|\overline{u}\phi\right), \quad M_v = -\frac{1}{J^2}\frac{v\sqrt{\gamma}}{\sqrt{u^2+v^2}}\frac{\partial}{\partial \eta}\left(|\overline{u}|\overline{u}\phi\right) \quad (14)$$

156   where $\phi = \sqrt{\dfrac{\gamma}{\alpha}}\dfrac{h^2}{R_\eta}k_{TS}$, $\overline{u} = \dfrac{ux_\xi + vy_\xi}{\sqrt{\gamma}}$, $\overline{v} = \dfrac{ux_\eta + vy_\eta}{\sqrt{\alpha}}$, R_η = the curvature radius of river

157   bend, k_{TS}= the lateral exchange coefficient due to circulation flow and can be calculated by

158
$$k_{TS} = 5\frac{\sqrt{g}}{\kappa C} - 15.6\left(\frac{\sqrt{g}}{\kappa C}\right)^2 + 37.5\left(\frac{\sqrt{g}}{\kappa C}\right)^3 \tag{15}$$

159 where $\kappa =$ Karman constant which is related to the sediment concentration (see below), $C =$

160 Chezy coefficient.

161
$$\kappa = 0.42[1 - 4.2(0.365 - S_v)\sqrt{S_v}] \tag{16}$$

162 where $S_v =$ the sediment concentration by volume.

163

164 The following key parameters need to be determined before the model can be applied for

165 simulation. .

166

167 *2.3. Suspended sediment carrying capacity*

168 Considering the effect of sediment concentration on Karman constant and silt deposition, Zhang

169 and Zhang（1992）presented a semi-empirical and semi-theoretical formula to calculate suspended

170 sediment carrying capacity based on the relationship between energy consumption of flow and the

171 power require to float sediment. Being verified by broad range of measured data in the Yellow

172 River, the formula has a high adaptability and can be used in the Upper Yellow River. The total

173 suspended sediment carrying capacity can be calculated as following:

174
$$S^* = 2.5\left[\frac{(0.0022 + S_v)\overline{U}^3}{\kappa\frac{\gamma_s - \gamma_m}{\gamma_m}gh\omega_s}\ln\left(\frac{h}{6D_{50}}\right)\right]^{0.62} \tag{17}$$

175 where $\overline{U} =$ vertical mean velocity; $D_{50}=$ medium diameter of bed material; $\gamma_s, \gamma_m =$ specific

176 gravity of sediment and muddy water, respectively; $\omega_s =$ group setting velocity. The units system

177 adopted is *kg, m* and *s*.

178

179   The group sediment carrying capacity S_L^* is obtained by multiplying S^* with p_L^* (the

180   graduation of group sediment carrying capacity):

$$S_L^* = p_L^* S^*$$ (18)

181

182   and p_L^* can be calculated by (Zhang, 1988):

$$p_L^* = w p_L + (1-w) p_{bL}^{'}$$ (19)

183

184   where P_L=graduation of suspended sediment at inlet; $p_{bL}^{'}$=related to the graduation of bed

185   material; w=weight factor, and its value ranges from 0.62 to 0.85 when the river bed is silted; from

186   0.64 to 0.86 when the river bed is scoured; and from 0.49 to 0.52 when the river bed keeps the

187   balance of erosion and deposition.

188

189   ***2.4. Sediment setting velocity***

190   The sediment setting velocity is a very important parameter in the sediment model. There are a lot

191   of formulae to calculate sediment setting velocity, among which the formula developed by Zhang

192   (1988) is one of the most representative formulae that are suitable for the sediment in the Yellow

193   River. According to Zhang (1988), the single grain sediment setting velocity in clean water can be

194   calculated as:

195
$$\omega_0 = \begin{cases} \dfrac{1}{25.6} \dfrac{\gamma_s - \gamma}{\gamma} g \dfrac{d^2}{v}, & \text{for } d \leq 0.1mm \\ 1.044 \sqrt{\dfrac{\gamma_s - \gamma}{\gamma} gd}, & \text{for } d \geq 4mm \\ \sqrt{\left(13.95 \dfrac{v}{d}\right)^2 + 1.09 \dfrac{\gamma_s - \gamma}{\gamma} gd} - C_1 \dfrac{v}{d}, & \text{for } 0.1mm < d < 4mm \end{cases}$$ (20)

196   where ω_0= the sediment setting velocity in clear water, d = the diameter of single grain sediment.

197

The sediment concentration in the Yellow River is usually high, which will affect the sediment

setting velocity. Therefore, the formula must be modified to take the effect of sediment

concentration into account. According to Zhang and Zhang (1992), the sediment setting velocity in

muddy water can be estimated as:

$$\omega = \omega_0 \left[\left(1 - \frac{S_v}{2.25\sqrt{d_{50}}} \right)^{3.5} (1-1.25S_v) \right]$$
(21)

where d_{50} is the medium diameter of a group of sediment.

204

2.5. Bedload sediment transport rate

Bedload transport rate is an important parameter that can be computed as following (Dou, *et al.*

1995):

$$g_{b,L} = K_0 \frac{\gamma_s U'\overline{U}^3}{\frac{\gamma_s - \gamma}{\gamma} g \omega_L C_0^2}$$
(22)

where $K_0=0.001$; $C_0=h^{1/6}/(ng^{1/2})$; $U' = \begin{cases} \overline{U} - U_c, & \overline{U} > U_c \\ 0, & \overline{U} \leq U_c \end{cases}$; U_c = the incipient velocity of

sediment, which can be calculated by:

$$U_c = 0.265\ln(\frac{11h}{\Delta})\sqrt{\frac{\gamma_s - \gamma}{\gamma} gd + 0.19\frac{\varepsilon_k + gh\delta}{d_{b50}}}$$
(23)

in which d_{b50} =the medium bedload diameter; $\varepsilon_k = 2.56\times10^{-6}m^3/s^2$; $\delta = 0.12\times10^{-6}m$;

Δ = roughness height of rive bed and can be determined as:

$$\Delta = \begin{cases} 0.5mm, & D_{50} \leq 0.5mm, \\ D_{50}, & D_{50} > 0.5mm. \end{cases}$$
(24)

215

216 *2.6. Recovering saturation coefficient*

217 Recovering saturation coefficient in (6) and (7) can be evaluated by (Wei *et al.* 1997)

218
$$\alpha_L = \begin{cases} 0.001/\omega_L^{0.3}, & S_L \geq S_L^* \\ 0.001/\omega_L^{0.7}, & S_L < S_L^* \end{cases} \tag{25}$$

219

220 **3. Numerical methods**

221 *3.1. Discretization of the governing equations*

222 The general governing equation (10) is discretized with finite volume method (FVM) (Versteeg

223 and Malalasekera 1995). The computational domain is rectangular in the BFC system and can be

224 easily divided into a series of small rectangles, as shown in Figure 1. Collocated grid system is

225 adopted in this study. In order to avoid the checkerboard pressure difference, momentum

226 interpolation method (Rhie and Chow, 1983) is used. The representative control volume is ΔV and

227 its centre is node P. The east, west, south and north faces of the control volume are *e, w, s* and *n*,

228 respectively. The east, west, south and north neighbor nodes of P are *E, W, S* and *N*, respectively.

229 Integrating Eq. (10) over the control volume ΔV yields:

230
$$\int_{\Delta V} \frac{\partial}{\partial t}(h\Phi)dV + \int_{\Delta V} \frac{1}{J}\frac{\partial}{\partial \xi}(hU\Phi)dV + \int_{\Delta V} \frac{1}{J}\frac{\partial}{\partial \eta}(hV\Phi)dV$$
$$= \int_{\Delta V} \frac{1}{J}\frac{\partial}{\partial \xi}(\frac{\alpha h\Gamma_\Phi}{J}\frac{\partial \Phi}{\partial \xi})dV + \int_{\Delta V} \frac{1}{J}\frac{\partial}{\partial \eta}(\frac{\gamma h\Gamma_\Phi}{J}\frac{\partial \Phi}{\partial \eta})dV + \int_{\Delta V} S_\Phi(\xi,\eta)dV \tag{26}$$

231

232 The first term (i.e. unsteady term, represented by I_t) on the left hand side is discretized by the

233 first order implicit scheme:

234
$$I_t \approx \frac{h_P\Phi_P - h_P^*\Phi_P^*}{\Delta t}J_P\Delta\xi\Delta\eta \tag{27}$$

235 where $\Delta t, \Delta\xi, \Delta\eta$ are time step, spatial steps in ξ and η directions, respectively. Subscript *

236   represents the variable of the last time step.

237

238   The second and third terms (i.e. convective terms, represented by I_C) on the left hand side are

239   discretized using an improved QUICK scheme developed by Hayase, *et al.* (1992). In this scheme,

240   a deferred correction method presented by Khosla and Rubin (1974) is used to improve the

241   QUICK scheme.

242
$$I_C = E_e - E_w + E_n - E_s \tag{28}$$

243   where

244
$$E_e = [|\,F_e,0\,|]\left(\Phi_P + \frac{1}{8}(3\Phi_E - 2\Phi_P - \Phi_W)^*\right) + [|-F_e,0\,|]\left(\Phi_E + \frac{1}{8}(3\Phi_P - 2\Phi_E - \Phi_{EE})^*\right) \tag{29}$$

245
$$E_w = [|\,F_w,0\,|]\left(\Phi_W + \frac{1}{8}(3\Phi_P - 2\Phi_W - \Phi_{WW})^*\right) + [|-F_w,0\,|]\left(\Phi_E + \frac{1}{8}(3\Phi_W - 2\Phi_P - \Phi_E)^*\right) \tag{30}$$

246
$$E_n = [|\,F_n,0\,|]\left(\Phi_P + \frac{1}{8}(3\Phi_N - 2\Phi_P - \Phi_S)^*\right) + [|-F_n,0\,|]\left(\Phi_N + \frac{1}{8}(3\Phi_P - 2\Phi_N - \Phi_{NN})^*\right) \tag{31}$$

247
$$E_s = [|\,F_s,0\,|]\left(\Phi_S + \frac{1}{8}(3\Phi_P - 2\Phi_S - \Phi_{SS})^*\right) + [|-F_s,0\,|]\left(\Phi_P + \frac{1}{8}(3\Phi_S - 2\Phi_P - \Phi_N)^*\right) \tag{32}$$

248   In which $[|\,F_e,0\,|] = max(F_e,0)$, $F_e = (hU\Delta\eta)_e$, $F_n = (hV\Delta\xi)_n$.

249

250   As a result, the scheme has not only the third order accuracy, but is also diagonally dominant and

251   can be easily programmed.

252

253   The first and second terms on the right hand side (i.e. diffusion terms, represented by I_D) are

254   discretized using the second order central difference scheme.

255
$$I_D = D_e(\Phi_E - \Phi_P) - D_w(\Phi_P - \Phi_W) + D_n(\Phi_N - \Phi_P) - D_s(\Phi_P - \Phi_S) \tag{33}$$

256   where

257
$$D_e = \left(\frac{\alpha \Gamma_\Phi h}{J}\right)_e \frac{\Delta \eta}{(\delta \xi)_e}, \ D_n = \left(\frac{\gamma \Gamma_\Phi h}{J}\right)_n \frac{\Delta \xi}{(\delta \eta)_n}.$$

258

259   The last term on the right hand side (the source term, represented by I_S) can be dealt with using

260   the following local linear method:

261
$$I_{S_\Phi} = I_{S_{\Phi C}} + I_{S_{\Phi P}} \Phi_P \tag{34}$$

262   where $I_{S_{\Phi P}} \leq 0$. As for momentum equations, the source terms are as following:

263
$$I_{S_{uC}} = -\Delta\xi\Delta\eta \left[gh(z_\xi y_\eta - z_\eta y_\xi) + \frac{\partial}{\partial \xi}\left(\frac{\beta \Gamma_u h}{J}\frac{\partial u}{\partial \eta}\right) + \frac{\partial}{\partial \eta}\left(\frac{\beta \Gamma_u h}{J}\frac{\partial u}{\partial \xi}\right) + \frac{1}{J}\frac{u\sqrt{\gamma}}{\sqrt{u^2+v^2}}\frac{\partial}{\partial \eta}\left(|\bar{u}|\bar{u}\phi\right)\right]$$

264
$$I_{S_{vC}} = -\Delta\xi\Delta\eta \left[gh(-z_\xi x_\eta + z_\eta x_\xi) + \frac{\partial}{\partial \xi}\left(\frac{\beta \Gamma_v h}{J}\frac{\partial v}{\partial \eta}\right) + \frac{\partial}{\partial \eta}\left(\frac{\beta \Gamma_v h}{J}\frac{\partial v}{\partial \xi}\right) + \frac{1}{J}\frac{v\sqrt{\gamma}}{\sqrt{u^2+v^2}}\frac{\partial}{\partial \eta}\left(|\bar{u}|\bar{u}\phi\right)\right]$$

265
$$I_{S_{uP}} = I_{S_{vP}} = -\frac{gn^2\sqrt{u^2+v^2}}{h^{1/3}}J_P\Delta\xi\Delta\eta.$$

266

267   The discretized equation of the general governing equation (10) using the above discretized

268   scheme is as following:

269
$$a_P\Phi_P = a_E\Phi_E + a_W\Phi_W + a_N\Phi_N + a_S\Phi_S + I_{S_{\Phi C}} + S^*_{ad} \tag{35}$$

270   where

271     $a_E = D_e + [|-F_e, 0|], a_W = D_w + [|F_w, 0|], \ a_N = D_n + [|-F_n, 0|], a_S = D_s + [|F_s, 0|],$

272     $a_P = a_E + a_W + a_N + a_S + F_e - F_w + F_n - F_s + a_P^* - I_{S_{\Phi P}}, b = a_P^*\Phi_P^* + I_{S_{\Phi C}},$

273     $a_P^* = \dfrac{h_P^*}{\Delta t}J_P\Delta\xi\Delta\eta, \ S^*_{ad} = (S^*_{ad})_e + (S^*_{ad})_w + (S^*_{ad})_n + (S^*_{ad})_s,$

274     $(S^*_{ad})_e = \dfrac{1}{8}(3\Phi_E - 2\Phi_P - \Phi_W)^*[|F_e, 0|] + \dfrac{1}{8}(3\Phi_P - 2\Phi_E - \Phi_{EE})^*[|-F_e, 0|],$

275     $(S^*_{ad})_w = \dfrac{1}{8}(3\Phi_P - 2\Phi_W - \Phi_{WW})^*[|F_w, 0|] + \dfrac{1}{8}(3\Phi_W - 2\Phi_P - \Phi_E)^*[|-F_w, 0|],$

276 $$(S^*_{ad})_n = \frac{1}{8}(3\Phi_N - 2\Phi_P - \Phi_S)^* [| F_n, 0 |] + \frac{1}{8}(3\Phi_P - 2\Phi_N - \Phi_{NN})^* [| -F_n, 0 |],$$

277 $$(S^*_{ad})_s = \frac{1}{8}(3\Phi_P - 2\Phi_S - \Phi_{SS})^* [| F_s, 0 |] + \frac{1}{8}(3\Phi_S - 2\Phi_P - \Phi_N)^* [| -F_s, 0 |].$$

278

279 Collocated grids SIMPLEC algorithm in body fitted coordinate system (Van Doormaal and

280 Raithby 1984) is used to solve the coupled problem of water level and velocities. The discretized

281 equations are five-diagonal, which can be solved using alternative direction tridiagonal matrix

282 algorithm (TDMA) (Versteeg and Malalasekera 1995).

283

284 *3.2. Semi-coupled scheme for sediment model*

285 In this study, a semi-coupled scheme is developed by combining the advantages of coupled and

286 decoupled schemes. In the process of long time simulation of sediment transport when river bed

287 changes slowly, the bed elevation change each time step has minimal impacts on flow field,

288 therefore, it is unnecessary to update the hydraulic elements each time step. Thus, in order to

289 reduce the computational cost, the hydraulic module runs intermittently while the sediment

290 module keeps running all the time. In the semi-coupled scheme, after the sediment module starts

291 to run, the hydraulic module will stop running for a certain number of time steps (for example,

292 1000-5000 time steps), then it will run again. After running for certain time steps (such as 60-120

293 time steps) to update the hydraulic elements, it will then stop running. The process is repeated

294 until the required accuracy is reached.

295

296 Let *t* be simulating time, *t0_flow* the initial simulation time for the flow module, *t1_flow* the flow

297 module working time each time, *t2_flow* the time interval between two adjacent times when flow

298   module is started, *t_max* the whole simulation time. The procedure of this semi-coupled scheme is

299   detailed as following:

300

301   *Algorithm of semi-coupled scheme:*

302   Step 1. If t≤t0_flow, only the flow module is running；

303   Step 2. If t0_flow< t<t_max, the sediment module is running.

304   Step 3. If t0_flow< t<t_max, and mod (t, t2_flow)<t1_flow, the flow and sediment modules are

305   running together；otherwise, only the sediment module is running.

306   Step 4. If t>t_max, stop.

307   where mod is a function which means modulus and mod (t, t2_flow) is the remainder when t is

308   divided by t2_flow. In this study, time step dt=12s, t0_flow=5h, t1_flow=1h, t2_flow=12h.

309   Numerical experiments indicate that the computational time of the semi-coupled scheme is about

310   60% of the coupled scheme.

311

312   *3.3. Boundary and initial conditions*

313   We choose two adjacent field measurements to verify the sediment model. The field measurements

314   were conducted on December 6, 2008 and on July 17, 2009, respectively. The time interval

315   between the two measurements is 203 days. Water discharge and sediment concentration are given

316   at the inlet based on values interpolated by field data measured on December 6, 2008 and on July

317   17, 2009. The turbulence kinetic energy (k) and its dissipation rate (ε) at the inlet are calculated

318   using empirical formulae (Rodi 1993). On the water outlet boundary, water level is specified based

319   on the values by interpolating the field data measured on December 6, 2008 and on July 17, 2009.

320   Other variables are dealt with using the fully developed condition. On the wall boundary, no-slip

321   boundary condition is applied. The velocity parallel to the river bank at the first cell is estimated

322   using standard wall function (Guo, et al. 2008).

323

324   In order to study the flow and sediment transport in the studied reach, four cases are used based on

325   discharge and sediment concentration at the inlet. The boundary conditions of the four cases are

326   presented in Table 1. Case 1 is set according to the field measured data on December 6, 2008,

327   while Case 2 is set according to the data measured on July 17, 2009. Case 3 and Case 4 are set

328   according to the hydrological data in the past years. Cases 1 and 4 represents the hydraulic

329   conditions of dry and flood seasons, respectively, while Cases 2 and 3 represents hydraulic

330   condition of wet season.

331

332   The initial values are based on field measured data on December 6, 2008, including the position of

333   cross-sections, water level, maximum water depth, average water depth, river width, average

334   velocity of 14 cross-sections (see Table 2). The initial water level at each grid is set as the same as

335   the water level at the outlet. u, v and S_L at each grid are set as zero, except for the grids at the inlet.

336   However, k and ε can not be set as zero, otherwise, the simulation process will stop unexpected or

337   be unstable. In the simulations, the initial values of k and ε are set as 0.1 m^2/s^2 and 0.0001 m^2/s^2,

338   respectively, based on the authors' experience.

339

340   The suspended and bedload sediment at the inlet section is divided into three groups with the

341   medium diameter being 0.0249 mm and 10 mm, respectively. The representative diameters and

17

342 related percentage for both the suspended and bedload sediment are listed in Table 3. The bed

343 material is divided into six groups, whose representative diameters and their percent content are

344 also presented in Table 3. The initial percentage contents of the suspended and bedload are set as

345 the same as the values at the inlet. Some representative diameters of the initial bed material of the

346 whole reach are: $d_{50} = 10$ mm, $d_m = 15.5$ mm, $d_{25} = 1$ mm, $d_{35} = 4$ mm, $d_{75} = 20$ mm,

347 $d_{90} = 70$ mm and $d_{95} = 100$ mm, where d_m = the mean diameter, d_a = the sediment diameter

348 that a% is less than that in the size gradation curve (a=25, 35,50,75,90,95).

349

350 *3.4. Mesh generation*

351

352 In the computational domain, along longitudinal direction (ξ-direction), 131 grids are assigned,

353 while along transverse direction (η-direction), 31 grids are set. Poisson equation method is used to

354 make body-fitted coordinate transformation and grid generation (Versteeg and Malalasekera

355 1995). The total number of grids and cells are 4991 and 4800, respectively. To better fit the

356 complex boundary, non-uniform meshes with arbitrarily spatially dependent size were used. This

357 allows for locally refining the concerned regions (e.g. near bends) with small meshes and has the

358 advantage of flexibly assigning meshes in the computational domain. Along transverse direction,

359 there are 30 cells, in which 5 non-uniform cells near left bank and near right bank, respectively.

360 The gird length of the 5 cells near bank increases from bank to interior. Figure 2 shows the mesh

361 distribution near banks and bends.

362

363 **4. Results and discussions**

364   ***4.1. Description of the computational domain and numerical simulation***

365   The Shapotou Reservoir in the Yellow River is located in Ningxia Hui Autonomous Region in

366   China. The studied reach is about 13.4km long, as shown in Figure 3. Twenty cross-sections (e.g.

367   SH1-SH15, SHJ1-SHJ5) are assigned in the studied reach, in which SH15 is the inlet, and SH1 is

368   the outlet. The studied reach consists of five bends: Bend A (from SH15 to SH13), Bend B (from

369   SH13 to SH11), Bend C (from SH11 to SH7), Bend D (from SH7 to SH2) and Bend E (from SH2

370   to SH1). Bends A and B are near the exit of the Heishan Gorge, where the river is deep and narrow,

371   and the current is rapid. The averaged water width at bend A and Bend B is about 135m with the

372   normal water level gradient being about 0.03%. Bends C, D and E are near the Shapotou Dam,

373   where the river is wide and shallow (the averaged water width is about 300 m), and the current is

374   slow. The normal water level gradient is about 0.006% .

375

376   In the simulation, the semi-coupled scheme in the 2D depth averaged RNG $k\text{-}\varepsilon$ sediment model is

377   applied. The software of Matlab 7.1 is used to program, and the numerical simulation is performed

378   on an IBM work station. The CPU of the work station is two cores Intel ® Xeon 2.0G Hz; the

379   memory is 4.0GB; the operation system is Ghost-Server2003 SP2. Typical numerical simulation

380   takes about 16 days.

381

382   ***4.2. Sediment setting velocity***

383   The sediment setting velocities of the six representative groups in the studied reach are calculated

384   by (19) and modified by (20), as listed in Table 4.

385

386   The sediment setting velocity is affected by the sediment concentration. Here we assume that the

387   sediment concentration is $S=10kg/m^3$ and the sediment concentration by volume is

388    $S_v=S/\rho_s=0.0038$ (ρ_s = density of sediment=$2650kg/m^3$). It is seen that the same sediment

389   concentration has different influence for the setting velocity of various grain size groups. The

390   correction rate is bigger for fine sediment than that for coarse sediment. In other words, sediment

391   concentration has larger effect on fine sediment than on the coarse one.

392

393   *4.3. Suspended sediment carrying capacity*

394   The suspended sediment carrying capacity is calculated using (16) and (17) for different group

395   sediment carrying capacity. Because the numerical results about suspended sediment carrying

396   capacity of the four cases are similar, only the result under the condition of Case 2 is presented in

397   this paper. Figure 4 shows the distribution of sediment concentration, total and group suspended

398   sediment carrying capacities along the centerline of the studied river reach. As shown in Figure 4,

399   both total and group sediment carrying capacities decrease along the way. It can also be found that

400   the carrying capacity of the second sediment group is the largest among the three sediment groups,

401   while the carrying capacity of the third sediment group is the smallest, which is consistent with the

402   sediment concentration of the three groups at the inlet.

403

404   *4.4. Bedload sediment transport rate*

405   In this study, four different methods are applied to calculate bedload sediment transport. The first

406   method (Method I) is to calculate group bedload transport rate by (22), then summing them to

407   obtain the total transport rate. The second method (Method II) is to calculate ω by (20) and (21),

408   where the representative sediment diameter (d) is chosen as d_{35}; then replacing ω_L with ω in

409   (21) to calculate the total bedload sediment transport rate. The third method (Method III) is the

410   same as Method II, except that the representative sediment diameter is d_m. The fourth method

411   (Method IV) is the same as Method II, except that d_{50} is chosen as the representative sediment

412   diameter.

413

414   From Table 5, it can be seen that the bedload transport rates calculated using the four methods are

415   different. Generally speaking, for non-uniform bedload sediment, it would be more accurate to

416   divide bedload sediment into several groups when computing its transport rate. Therefore, the

417   result calculated using Method I is the most reliable. The result calculated by Method II is closer

418   to the result of Method I, indicating that the transport rate of non-uniform bedload sediments can

419   be calculated using the formula for computing the transport rate of uniform bedload sediments

420   when the representative sediment diameter is chosen as d_{35} for the flow and sediment conditions

421   investigated here This result is consistent with the conclusion of Einstein (Zhang, 1988).

422

423   *4.5. Comparison between measured and calculated velocities*

424   Figure 5 shows the comparison of the simulated and field measured (on July 16 2009) depth

425   averaged velocities on three selected cross-sections, i.e. SH7, SH5, SHJ2, which are near the inlet,

426   apex, and outlet of Bend D, respectively. Figure 5(1) also shows the comparison of the depth

427   averaged velocities calculated using two methods: Simulation 1 and Simulation 2. In Simulation 1,

428   the circulation flow is not taken into account, while this has been taken into account in Simulation

429   2. It is seen that the simulated velocity using the second approach is better compared to the

430 measured data than that using the first method, indicating that the modified plane 2D RNG k-ε

431 model is capable of simulating the effect of the circulation flow in natural rivers. In general, good

432 agreements between simulated and field measured velocities at three cross sections are obtained.

433

434 *4.6. Comparison between measured and calculated river bed deformation*

435 Figure 6 is the plot of the simulated and field measured (on July 17 2009) bed elevation along the

436 longitudinal direction. It is seen that the simulated bed elevation is in good agreement with the

437 measured data. From SH11 to SH9, the river bed is scoured, while from SHJ5 to SH2, the river

438 bed is deposited. The deposit thickness varies significantly from SH2 to SH5 with the largest

439 deposition taking place in SH2 (where the average deposit thickness is over 1 m), while little

440 deposit takes place at SH5 (where the average deposit thickness is only about 0.01 m).

441

442 In Figure 7, the measured and the simulated bed elevations at three typical cross sections are

443 plotted. The three cross sections are SH10, SHJ5 and SH7, which are near the inlet, the bend apex,

444 and the outlet of Bend C, respectively. It is seen from Figure 7 that the simulated bed elevation

445 agrees well with the measured data on these cross sections, indicating that the 2D depth averaged

446 RNG k-ε sediment model can reasonably simulate the bed deformation in the studied reach. The

447 bed on SH10 is scoured as a whole except some small areas near the river banks. The bed near the

448 left bank of SHJ5 and SH7 is deposited and the bed near the right bank of the two cross-sections is

449 scoured. Because the left bank is the convex bank，while the right bank is the concave bank in

450 Bend C, the above phenomenon is in consistence with the general rule of sediment transport in a

451 bend.

452

453   *4.7.   Suspended sediment transport*

454   Figure 8 shows the distribution of suspended sediment concentration along the centerline of the

455   studied reach under the condition of Case 2 with the sediment concentration at the inlet being set

456   as 0.51, 3.53, 10 and 20 kg/m^3, respectively. From Figure 8, it is seen that the suspended sediment

457   concentration in the studied reach increases with increasing the suspended sediment concentration

458   at the inlet. As the river of the studied reach becomes wider and shallower as the flow moves

459   downstream, the flow becomes slower and the sediment carrying capacity becomes weaker

460   accordingly along the way, leading to the decrease of the suspended sediment concentration along

461   the way.

462

463   *4.8. The effect of discharge on river bed deformation*

464   In order to investigate the effect of the discharge at the inlet on the bed deformation, numerical

465   simulations were conducted for four cases. The conditions of the four cases are shown in Table 1

466   except that the sediment concentration at the inlet is set as 3.53kg/m^3. Figure 9 shows the

467   simulated bed elevation after 10 days development for all four cases. The bed is deposited near the

468   inlet for Cases 1 and 2, while the bed is scoured near the inlet under the condition of Cases 3 and 4.

469   The reason is that the average velocities for the Cases 1 and 2 are small, and the suspended

470   sediment capacities are smaller than the sediment concentration. As a result, the bed is deposited

471   near the inlet. However, after flow moves a certain distance, a balance between deposition and

472   scour is reached. The position of balance is about 9.5km from the inlet for Case 1, and it is near

473   SH5; while for Case 2, it is about 10.5km from the inlet and near SH4. The discharges and average

474   velocities of the Cases 3 and 4 are larger, and the suspended sediment capacities of the two cases

475   are larger than sediment concentration. Therefore, the bed is scoured near the inlet. Similar to

476   Cases 1 and 2, a balance between deposition and scour is reached after the flow moves a certain

477   distance away from the inlet. For Case 3, the position is about 4.5km from the inlet and near SH10;

478   while for Case 4, the position is about 6km from the inlet and near SHJ5. From above analysis, it

479   can be concluded that the discharge at the inlet has significant influence on the bed deformation

480   near the inlet. However, after the flow moves a certain distance, the influence becomes weaker and

481   weaker.

482

483   *4.9. River bed deformation caused by bedload sediment*

484   Though the bed deformation is mainly caused by the suspended sediment transport, the bedload

485   sediment transport can also have significant effect on the bed deformation for some certain

486   situations. To investigate the effect of bedload sediment transport on the river bed deformation, the

487   numerical simulation is conducted for four cases with the same suspended sediment concentration

488   at the inlet being 3.53kg/m^3. Figure 10 shows the percentage of the absolute thickness deposited or

489   scoured by suspended and bedload sediments for four typical cases after 10 days development,

490   respectively. It can be seen that the thicknesses deposited or scoured due to the suspended or

491   bedload sediment transport is quite different. In Cases 1 and 2, the percentage of bed deformation

492   caused by bedload sediment is less than 1%, which is negligible. In Case 3, the percentage is less

493   than 3% and is still very small and can be neglected. In Case 4, however, the percentage is about

494   10%, which can not be neglected. Therefore, it can be concluded that the bed deformation caused

495   by bedload sediment can be neglected when the discharge at the inlet is small (less than 1500m^3/s

496 in this study). When the discharge at the inlet is larger (more than 2000m^3/s in this study),

497 however, the bed deformation caused by bedload sediment reaches a certain level and has to be

498 taken into account. .

499

500 *4.10. The variation of effective bed material granularity*

501 Bed material becomes finer or coarser when the bed is deposited or scoured and it is worth of

502 investigating. Because the simulated results for four cases are similar, only the numerical result of

503 Case 4 is presented and discussed in this paper. Under the condition of Case 4, numerical

504 simulations were conducted for the sediment concentration at the inlet (S_{in}) being 0.51kg/m^3 and

505 10kg/m^3, respectively.

506

507 Figure 11 shows the variation of effective bed material granularity along the river flow direction

508 after 20 days. In Figure 11, the axis x is the distance from the inlet, and the axis y is the percentage

509 of each group effective bed materials. The percentage of the initial bed material for the six groups

510 is 0.2%, 3.8%, 17.9%, 12.7%, 36.5%, 28.9%, respectively, as shown by the dash line in Figure 11.

511

512 When S_{in} = 0.51kg/m^3, the river bed is scoured as a whole and the bed material size gradation is

513 changed after 20 days' scouring. In Figure 11(a), it is seen that the percentage of the first three

514 groups (Groups 1-3) of bed material decreased compared with the initial value, especially for

515 Groups 2 and 3. The decreasing tendency becomes weaker with the distance and reaches the

516 minimum at the distance from the inlet. Meanwhile, the percentage of the last three groups

517 (Groups 4-6) of bed material increased compared with the initial value. The increasing tendency

518   also becomes weaker with the distance and reaches the minimum at the distance of 8.5km from the

519   inlet (near SH6). And after SH6, the bed material granularity is almost not changed for all of the 6

520   groups. This means that bed becomes coarser when the bed is scouring. However, after SH6, the

521   sediment concentration at the inlet has little influence to the bed deformation and variation of bed

522   material granularity, as shown by Figure 9 and Figure 11.

523

524   When S_{in}=10kg/m^3, the situation is different and complicated. As shown in Figure 11(b), the bed

525   material percentage of Groups 1-3 increases, while the percentage of Groups 4-6 decrease as a

526   whole compared with the initial value. In Figure 11(b), it can also be found that the percentage of

527   the first three groups of the bed material increases with the distance and reaches the maximum

528   near SH6. The percentage of these groups then decreases with the distance. To the contrary, the

529   last three groups of the bed material decreases with the distance and reaches the minimum at about

530   8.5 km from the inlet and increases again to the outlet. This means that the river bed becomes finer

531   compared with the initial value when it is deposited. Similar to the condition when S_{in}=0.51 kg/m^3,

532   after SH6, the sediment concentration at the inlet has little influence to the bed deformation and

533   variation of bed material granularity.

534

535   **5. Conclusions**

536   In this study, a 2D depth averaged RNG k-ε sediment model including the effects of secondary

537   currents is developed, which considers the effects of the non-uniform suspended and bedload

538   sediment transport on the bed deformation. In the model, the variation of effective bed material

539   size distribution is included. A semi-coupled scheme is developed by combining the coupled and

540   decoupled schemes to improve the accuracy of the numerical simulation (compared with the

541   decoupled scheme) and save computational time (compared with the coupled algorithms).

542   Numerical simulations have been performed for four typical cases to investigate the sediment

543   transport and bed deformation in the upper reach of the Yellow River. Comparison between the

544   numerical results and field measurements indicates that the 2D depth averaged RNG k-ε sediment

545   model can reasonably simulate the sediment transport and the resultant bed deformation of rivers

546   with continuous bends. River bed deformation induced by suspended and bedload sediment

547   transport has been investigated. It is found that the bed deformation caused by bedload sediment

548   transport can be neglected when the discharge at the inlet is small (less than $1500\text{m}^3/\text{s}$ in this

549   study). The results also show that the discharge at the inlet has significant effect on the bed

550   deformation near the inlet. The influence, however, becomes weaker as the flow moves

551   downstream.

552

553   The variation of effective bed material granularity has been examined. It is concluded that the bed

554   material granularity becomes finer when the bed is deposited. When the bed is scoured, the bed

555   material granularity becomes coarser. The bed material granularity becomes finer along the way in

556   the studied reach no matter it is deposited or scoured. The sediment concentration at the inlet has

557   significant influence for bed material granularity near the inlet. However, the influence becomes

558   weaker with the distance from the inlet.

559

560   **6. Acknowledgements**

566   **7. References**

567   Dou, G.R., Dong, F.W., Dou, X.P., Li, T.L., 1995. Mathematical modeling of sediment transport in

568   estuaries and coastal regions. *Science in China(Series A)*, 38 (10):1251-1260.

569   Duan, J.G., Nanda, S.K., 2006. Two-dimensional depth-averaged model simulation of suspended

570   sediment concentration distribution in a groyne field. *Journal of Hydrology*, 327, 426-437.

571   Duan, J.G., Julien, P.Y., 2010. Numerical simulation of meandering evolution. *Journal of*

572   *Hydrology*, 391: 34-46.

573   Falconer, R.A. 1992. Flow and water quality modelling in coastal and inland water. *J. Hydraul.*

574   *Res*., 30, 437-452.

575   Guo, Y.K., Wang, P.Y., Zhou, H., 2007. Numerical modelling of the flow past irregularities in a

576   pressure conduit, *ASCE J. Hydr. Eng.,* 133(6): 698-702.

577   Guo, Y.K., Zhang, L.X., Shen, Y.M., Zhang, J.S., 2008. Modeling study of free overfall in a

578   rectangular channel with strip roughness, *ASCE J. Hydr. Eng.,* 134(5): 664–667.

579   Guo, Y.K., Wu, X.G., Pan, C.H., Zhang, J., 2012. Numerical Simulation of the Tidal Flow and

580   Suspended Sediment Transport in the Qiantang Estuary, *ASCE Journal of Waterway, Port, Coastal*

581   *and Ocean Engineering,* 138: 192-203.

582   Hayase, T., Humphrey, J.A.C., Greif, G., 1992. A consistently formulated QUICK scheme for fast

583   and stable convergence using finite volume iterative calculation proceeding. *J. Comput. Phys.*,

584   98:108-118.

585   Hung, M.C., Hsieh, T,Y,, Wu, C.H., Yang, J.C., 2009. Two-Dimensional nonequilibrium

586   noncohesive and cohesive sediment transport model. *J. Hydr. Eng.(ASCE)*, 135(5) : 369-382

587   Jing, H.F., Guo, Y.K., Li, C.G, Zhang, J.S., 2009. Three-dimensional numerical simulation of

588   compound meandering open channel flow by the Reynolds stress model. *Int. J. Numer. Mech.*

589   *Fluids,* 59, 927-943.

590   Jing, H.F., Li, C.G, Guo, Y.K., Xu, W.L., 2011. Numerical simulation of turbulent flows in

591   trapezoidal meandering compound open channels. *Int. J. Numer. Mech. Fluids,* 65, 1071-1083.

592   Khosla, P.K., Rubin, S.G., 1974. A diagonally dominant second order accurate implicit scheme.

593   *Computer & Fluids,* 2:207-209.

594   Li, S.S., Millar, R.G., 2011. A two-dimensional morphodynamic model of gravel-bed river with

595   floodplain vegetation. *Earth Surface Process & Landforms,* 36(2): 190-202.

596   Lien, H.C., Hsieh, T.Y., Yang, J.C., Yeh, K.C., 1999. Bend-flow simulation using 2D

597   depth-averaged model. *ASCE J. Hydr. Eng.*, 125, 1097-1108.

598   Nagata, N., Hosoda, T., Muramoto, Y., 2000. Numerical analysis of river channel processes with

599   bank erosion. *ASCE J. Hydr. Eng.*, 126 (4): 243 -252.

600   Rhie, C.M., Chow, W.L., 1983. A numerical study of the turbulent flow past an isolated airfoil

601   with trailing edge separation. *AAIA J.,* 21:1525-1532.

602   Rodi, W., 1993. *Turbulence models and their application in hydraulics: A state-of-the-art review,*

603   *3rd Ed.,* Balkema, Rotterdam, the Netherlands.

604   Serrano-Pacheco, A., Murillo, J., Garcia-Navarro, P., 2012. Finite volumes for 2D shallow-water

605   flow with bed-load transport on unstructured grids, *Journal of Hydraulic Research,* 50(2):

606   154-163.

607   Van Doormaal, J.P., Raithby, G.D., 1984. Enhancement of SIMPLE method for predicting

608   incompressible fluid flows. *Numer. Heat Transfer*, 7(2): 147-163.

609   Versteeg, H.K., Malalasekera, W., 1995. *An introduction to computational fluid dynamics*.

610   Addison Wesley Longman Limited, England.

611   Wei, Z.L., Zhao, L.K., Fu, X.P., 1997. Research on mathematical model for sediment in Yellow

612   River, *J. Wuhan University of Hydro. & Electric Eng*., 30(5):21-25.

613   Yakhot, V., Orzag, S.A., 1986. Renomalization group analysis of turbulence: basic theory. *J.*

614   *Scient Comput.*, 1, 3-11.

615   Zhang, H.W., Zhang, Q., 1992. Formula of Sediment Carrying Capacity of the Yellow River .

616   *Yellow River,* (11):6-9.

617   Zhang, R.J., 1988. *River Sediment Dynamics(the second edition)*. Beijing: Water Conserversy and

618   Hydropower of China.

619

639

Table 1   Boundary conditions of four cases

Cases	Inlet					Outlet
	$Q\ (m^3/s)$	$U\ (m/s)$	$S\ (kg/m^3)$	$k(m^2/s^2)$	$\varepsilon(m^2/s^3)$	$z(m)$
Case 1	513.50	1.0398	0.51	0.0121	0.0005	1239.68
Case 2	930.00	1.5405	3.53	0.0269	0.0013	1240.65
Case 3	1500.00	1.8098	10	0.0378	0.0016	1241.50
Case 4	2000.00	2.0579	20	0.0492	0.0020	1242.00

640

641

642

Table 2.   Some data measured on December 6, 2008

Cross section No.	Distance from the inlet /km	Water level /m	Maximum water depth /m	Average water depth/m	River width /m	Average velocity /m/s
SH2	12.52	1240.51	8.58	6.19	212.10	0.35
SH3	11.71	1240.53	6.10	5.31	269.50	0.31
SHJ2	11.26	1240.54	5.78	5.40	267.50	0.33
SH4	10.58	1240.58	6.70	5.47	215.50	0.49
SHJ3	10.14	1240.76	8.43	5.28	214.90	0.52
SH5	9.68	1240.79	8.47	5.07	228.00	0.56
SH6	8.70	1240.82	7.14	4.47	295.40	0.44
SHJ4	8.20	1240.86	6.23	4.69	259.30	0.49
SH7	7.60	1240.88	6.49	4.75	234.20	0.38
SH8	6.75	1240.90	7.34	5.44	221.70	0.35
SHJ5	6.25	1240.91	6.04	4.72	245.90	0.53
SH9	5.55	1241.02	6.45	4.84	175.90	0.54
SH10	4.69	1241.27	13.68	7.67	115.00	0.44
SH11	3.70	1241.38	6.29	4.65	155.90	0.81

643

644

645

646   Table 3 The initial percent content of bed materials, suspended sediment and bedload

group	1	2	3	4	5	6
diameters /mm	0.01	0.05	0.25	2	10	40
Bed materials /%	0.2	3.8	17.9	12.7	36.5	28.9
Suspended sediment /%	38	53	9			
Bedload /%				38.3	31.3	30.4

647

648

649

650

<div align="center">Table 4　Sediment group setting velocity of six groups</div>

Sediment grain size /mm	Single setting velocity (cm / s)	Group setting velocity (cm / s)	Correction rate (%)
0.01	0.0062	0.0059	4.92
0.05	0.1570	0.1522	3.14
0.25	1.6142	1.5877	1.69
2	5.8798	5.8277	0.91
10	13.3038	13.2164	0.67
40	26.6075	26.4575	0.58

651

652

653   Table 5 Bedload sediment transport rate at the centerline of some cross sections calculated by
654   four methods under the condition of Case 2 (unit: kg/ms)

Cross sections	Method I	Method II	Method III	Method IV
SH1	0.0018	0.0023	0	0
SH2	0.0006	0.0003	0	0
SHJ2	0.0013	0.0014	0	0
SHJ3	0.0003	0	0	0
SH6	0.001	0.001	0	0
SH7	0.0033	0.0046	0	0
SHJ5	0.0028	0.0037	0	0
SH10	0.0111	0.013	0.0001	0.0034
SH12	0.0499	0.0523	0.0128	0.0228
SH14	0.0415	0.0439	0.0099	0.0184

655

656

657
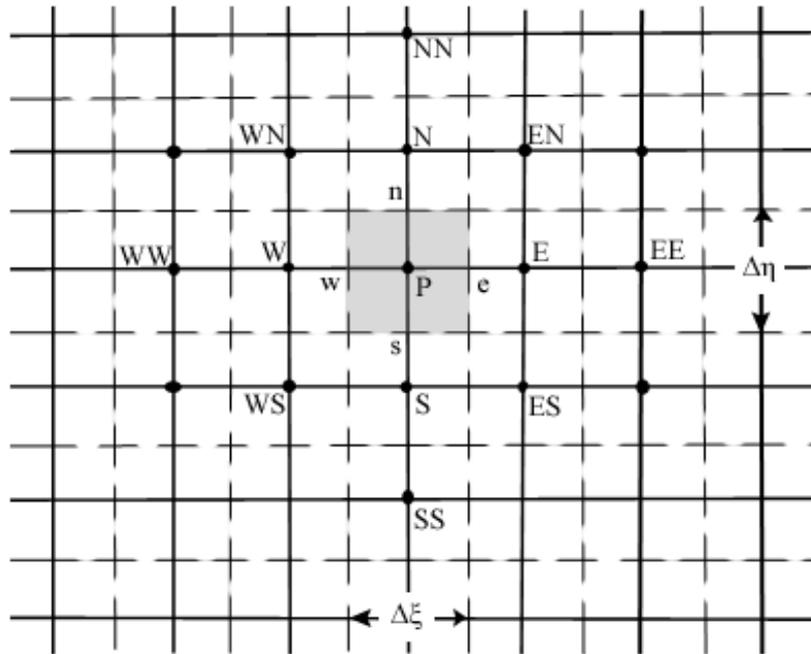
658

659   Figure 1 The grid and control volume of finite volume method

660
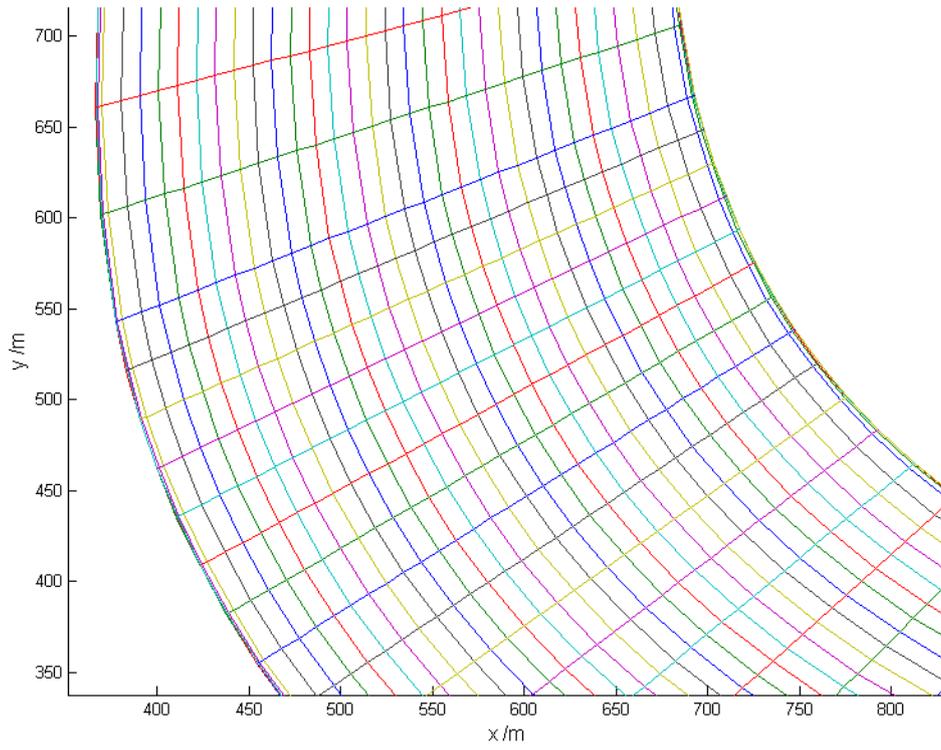
661

662   Figure 2 Meshes distribution near banks and bends

663

664
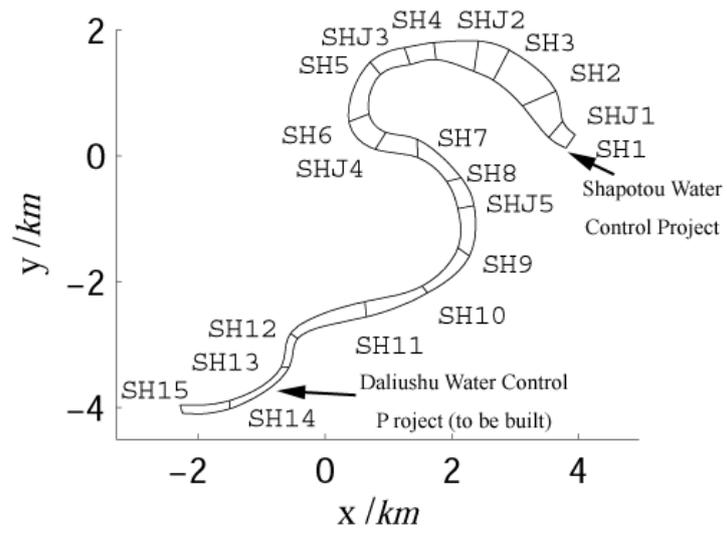
Figure 3 Plane view of Shapotou reservoir (The flow is in from SH15 and out from SH1, and the

direction of axis x is consistent with the east)

665

666

667

668
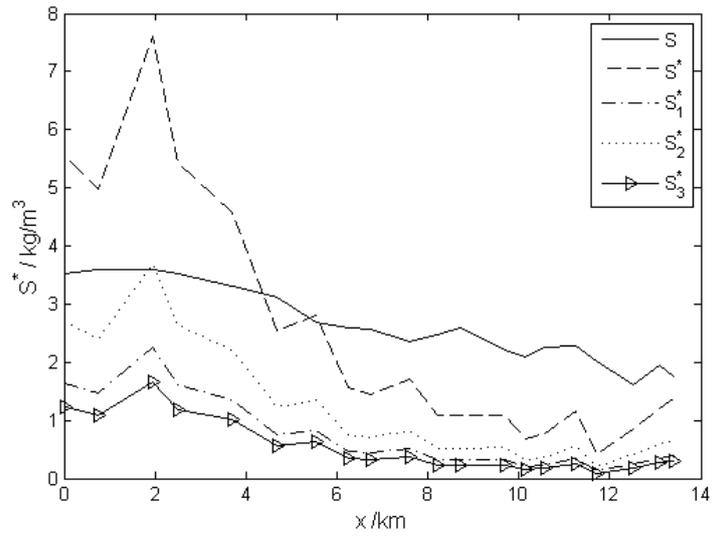
669

670   Figure 4 The distribution of total and group suspended sediment capacities(Case 2)
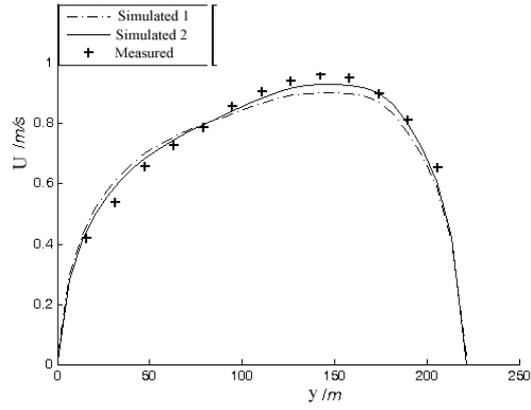
671

672   (1) SH7
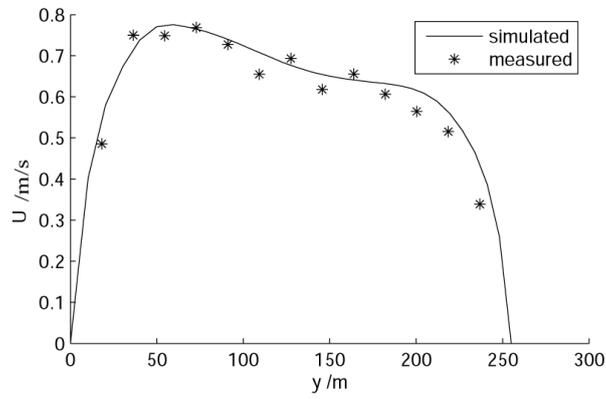
673

674   （2） SH5
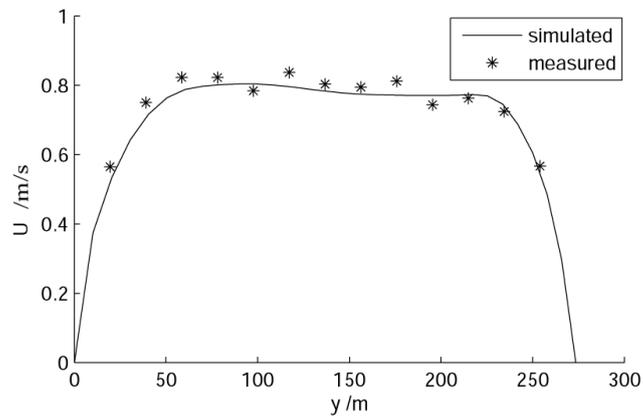
675

676   (3) SHJ2

677   Figure 5.   Comparison of simulated and measured depth averaged velocities on three typical

678   cross-sections

679
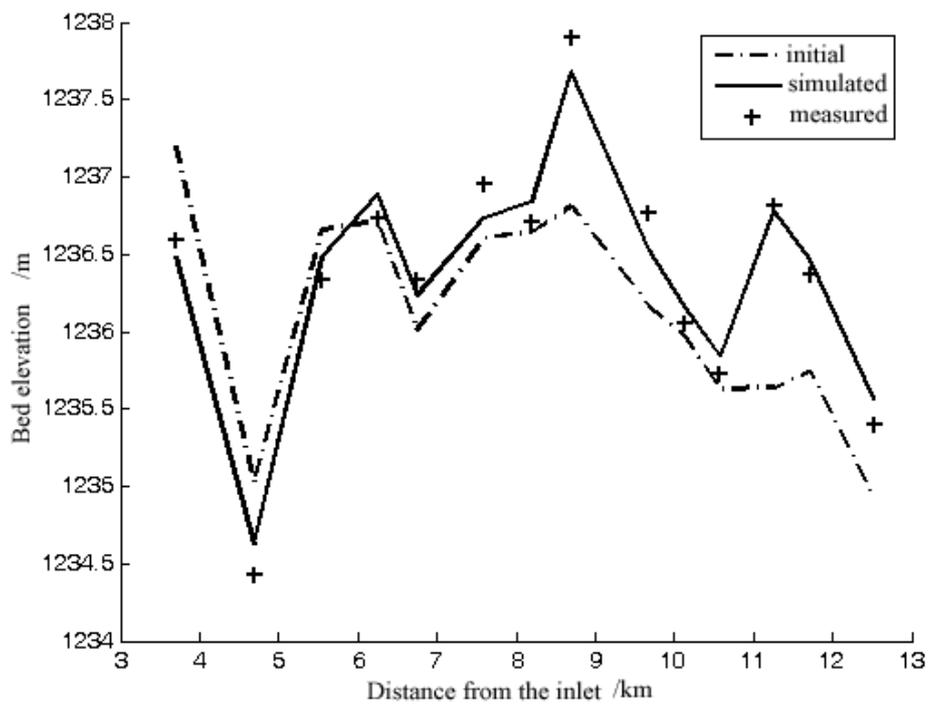
680

681   Figure 6 Comparison of simulated and measured bed elevation along the longitudinal direction
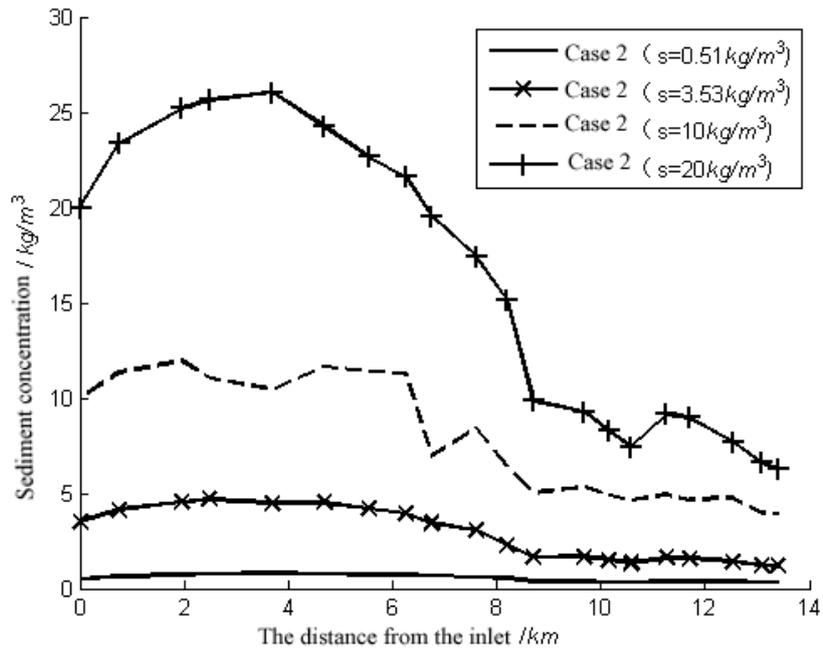
682
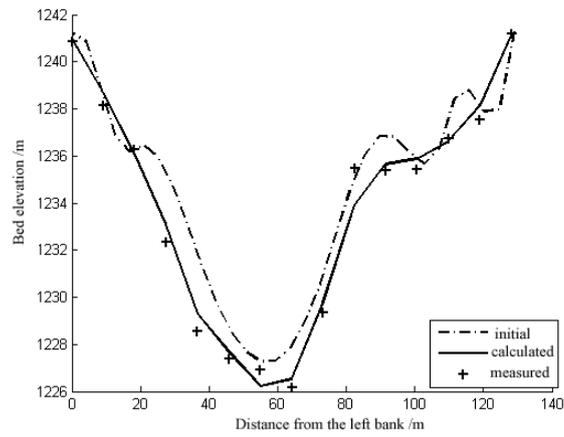
（1）SH10
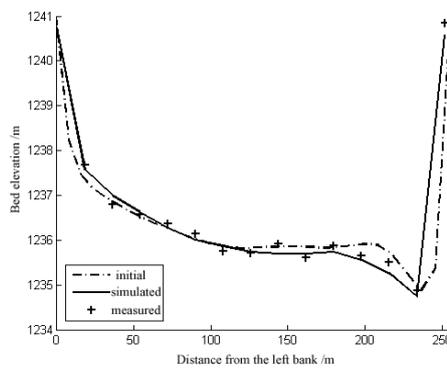
684

685   （2）SHJ5
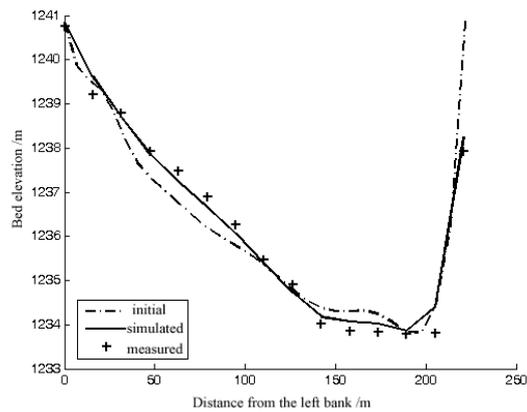
686

687   （3）SH7

688   Figure 7 Comparison of the measured and the simulated bed elevations on three typical cross
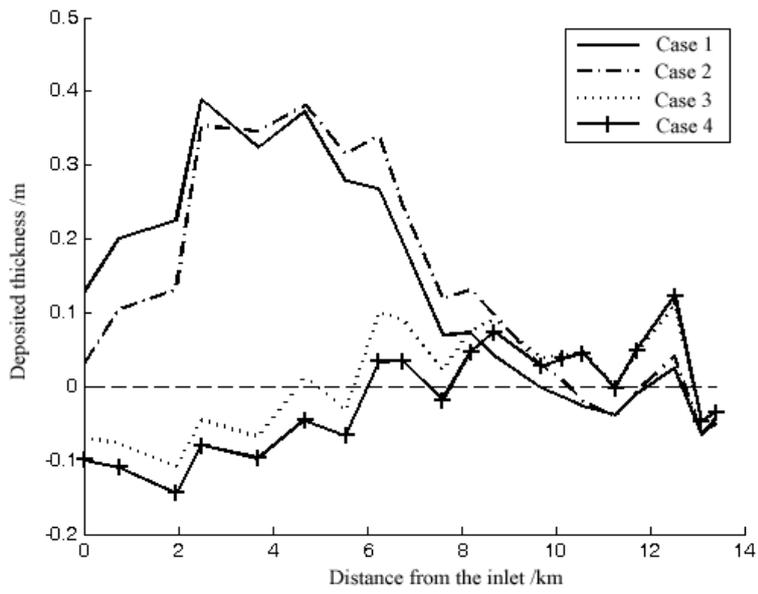
689   sections

690

691

692   Figure 8 Distribution of suspended sediment concentration along the centerline of the studied

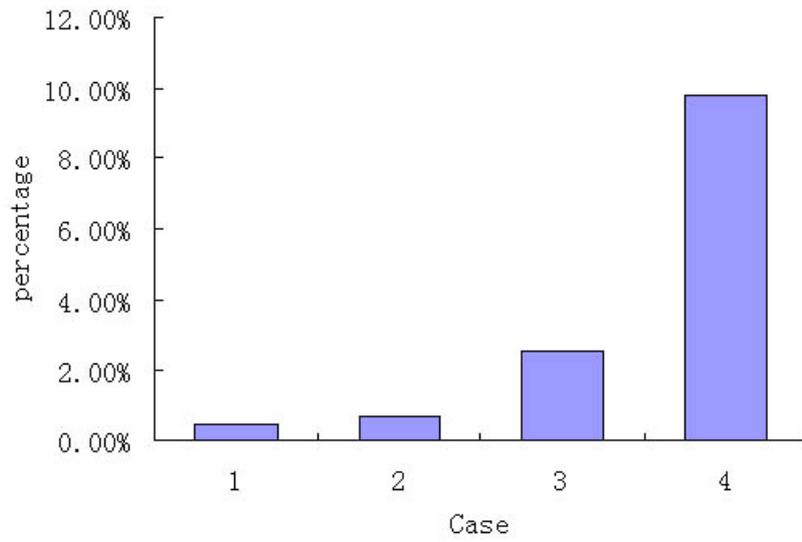693   reach under the condition of Case 2

694

695

696   Figure 9   Comparison of the simulated bed deformations among the four cases with the same

697   sediment concentration（3.53kg/m^3）at the inlet
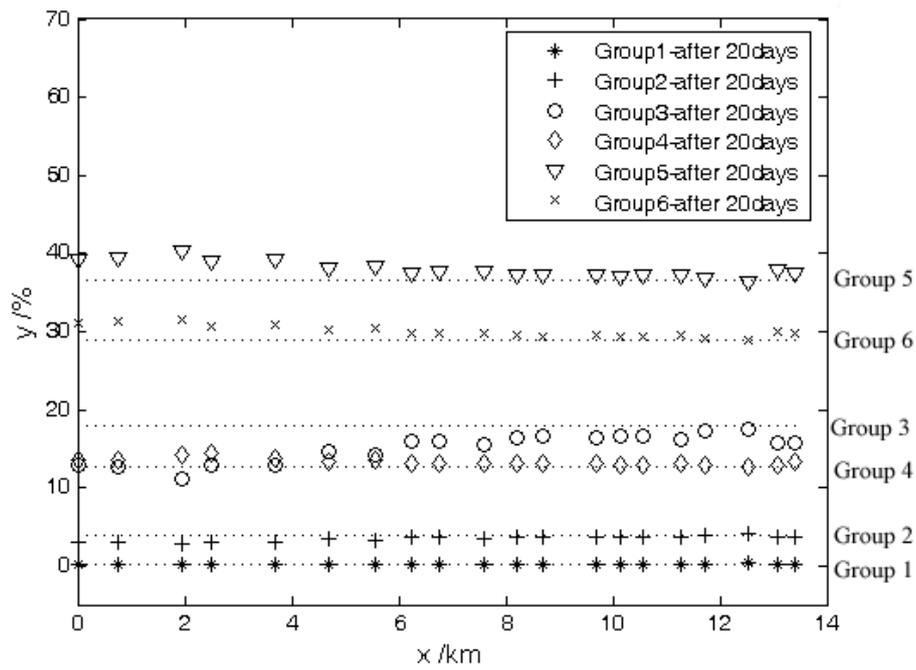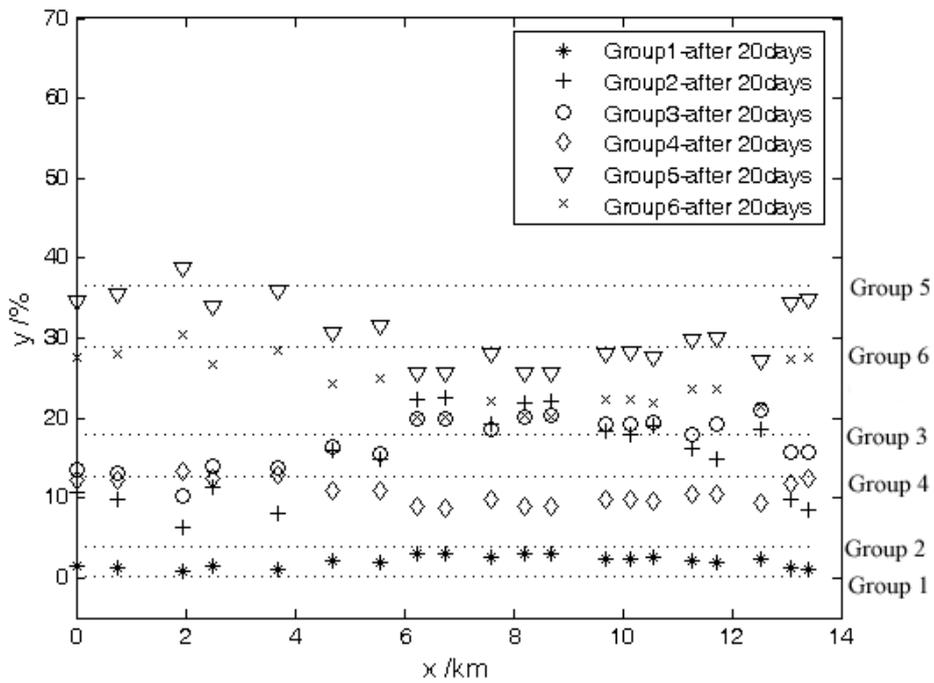
698

699　　　　　Figure 10 Percentage of bed deformation caused by bedload sediments in four cases

700

701

702

703   (a) $S_{in}=0.51kg/m^3$

704
705   (b) $S_{in}=10kg/m^3$

706   Figure 11 The variation of effective bed material composition after 20 days